

Jamming Detection in MIMO-OFDM ISAC Systems Using Variational Autoencoders

Luca Arcangeloni, Enrico Testi, and Andrea Giorgetti
CNIT/WiLab, DEI, University of Bologna, Italy
Email: {luca.arcangeloni2, enrico.testi, andrea.giorgetti}@unibo.it

Abstract—This paper introduces a novel unsupervised jamming detection framework designed specifically for monostatic multiple-input multiple-output (MIMO)-orthogonal frequency-division multiplexing (OFDM) radar systems. The framework leverages echo signals captured at the base station (BS) and employs the latent data representation learning capability of variational autoencoders (VAEs). The VAE-based detector is trained on echo signals received from a real target in the absence of jamming, enabling it to learn an optimal latent representation of normal network operation. During testing, in the presence of a jammer, the detector identifies anomalous signals by their inability to conform to the learned latent space. We assess the performance of the proposed method in a typical integrated sensing and communication (ISAC)-enabled 5G wireless network, even comparing it with a conventional autoencoder.

Index Terms—Variational autoencoder, generative AI, jamming detection, joint sensing and communication, anomaly detection, radar.

I. INTRODUCTION

IN the context of 6G, the emerging paradigm of integrated sensing and communication (ISAC) systems is expected to revolutionize applications such as traffic monitoring and autonomous driving, while also enhancing urban safety [1]–[3]. Despite these advantages, ISAC systems are sensitive to a range of traditional radar security threats (e.g., advanced radar electronic countermeasure (ECM)), which are designed to deceive the sensing systems [4]. Among those attacks, the deceptive jamming technique known as digital radio frequency memory (DRFM) is particularly significant, as it enables precise scaling and delaying of intercepted radar waveforms by the jammer. Moreover, the global DRFM market is projected to experience substantial growth due to the widespread adoption of artificial intelligence (AI). A deceptive jammer can exploit information about signals transmitted by the base station (BS) to mimic the behavior of a typical network user equipment (UE). For example, common pilot/reference signals proposed for integrating sensing capabilities into communication networks [5]–[7] might already be known to intruders, potentially jeopardizing network security.

This work was supported by the European Union under the Italian National Recovery and Resilience Plan (NRRP) of NextGenerationEU, partnership on “Telecommunications of the Future” (PE00000001 - program “RESTART”). The authors are with the Department of Electrical, Electronic, and Information Engineering “Guglielmo Marconi” (DEI), CNIT, University of Bologna, Italy (e-mail: {luca.arcangeloni2, enrico.testi, andrea.giorgetti}@unibo.it).

In radar literature, several approaches have been proposed to detect a deceptive jammer. Classic methods exploit likelihood-based algorithms that model the echo signals and adopt the generalized likelihood ratio test (GLRT) [8], [9]. They employ a two-block approach to unravel a multiple hypothesis test: initially, the presence of a target is detected; then, a second test is conducted to distinguish between an actual radar target and a false one. While such likelihood-based methods rely on prior information such as the statistical distribution of the channel and that of the clutter, in [10] jamming detection and classification are performed by means of a decision tree and a support vector machine (SVM), fed with a set of features extracted directly from the received signal. In [11], the authors propose electronic counter-countermeasures (ECCM) schemes for orthogonal frequency-division multiplexing (OFDM) radar that improve local signal-to-interference plus noise ratio (SINR), optimize initial phases to resist deception jamming, and develop waveform optimization methods to minimize jamming energy. In [12], the authors propose a power optimization strategy for multiple radar systems to counteract deception jamming in multi-target tracking tasks. They derive the posterior Cramér-Rao lower bound for deception range, which is crucial for distinguishing between physical and false targets. Using this metric, they introduce a method for false target discrimination and formulate a power optimization problem aimed at optimizing both tracking accuracy and discrimination performance. Recently, the introduction of AI techniques in the field of wireless communications gave impetus to the development of neural network (NN)-based jamming detectors [13], [14]. In [15], an ensemble convolutional neural network (CNN) with transfer learning is proposed to recognize a variety of deceptive jammers. In particular, a time-frequency dataset is constructed using the short-time Fourier transform. Then, features such as the real and imaginary parts, modulus, and phase are extracted to build different subdatasets. These subdatasets serve as the input for classifiers in the ensemble model.

In this work, we present a novel unsupervised jamming detection framework tailored for a monostatic multiple-input multiple-output (MIMO)-OFDM radar system. The framework utilizes the echo signals captured at the BS and employs the variational autoencoder (VAE), a generative latent variable model adept at learning latent data representations [16]. The contributions of this work are the following:

- We propose a jamming detection framework that, starting from the echo signals acquired by the BS and leveraging the latent space identification capability of VAEs is able to detect the presence of an intruder in a MIMO-OFDM system. The detector is trained on a dataset consisting of received echoes from a real target in the absence of jamming, allowing the VAE to learn the optimal latent representation of the data. During testing, when the jammer is present, the detector identifies the anomalous signal by its incompatibility with the learned latent space.
- To evaluate the performance of the proposed solution, we investigate a case study consisting of a 5G wireless network employing an ISAC system in presence of a deceptive jammer.
- Finally, the performance of the VAE-based jamming detector is compared with that of a conventional autoencoder (AE), which has been carefully designed and trained to achieve its optimal performance.

Throughout the paper, capital and lowercase boldface letters denote matrices and vectors, respectively. With $v_{i,j}$, $\mathbf{v}_{i,:}$, and $\mathbf{v}_{:,j}$, we represent, respectively, the element, the i th row, and the j th column of the matrix \mathbf{V} . $X \sim \mathcal{U}(a, b)$ denotes a uniform distributed random variable (r.v.) between a and b . $X \sim \mathcal{N}(\mu, \sigma^2)$ denotes a Gaussian r.v. with mean μ and variance σ^2 , and $Z \sim \mathcal{CN}(0, \sigma^2)$ denotes a zero-mean circularly symmetric complex Gaussian r.v. with variance σ^2 . We denote the expectation operator by $\mathbb{E}[X]$. $(\cdot)^\top$ and $(\cdot)^*$ denote the transpose and the conjugate operations, respectively.

II. SYSTEM MODEL

Let us consider the monostatic MIMO-OFDM system depicted in Fig. 1, which consists of transmitter and receiver antenna arrays with N_T and N_R elements, respectively, used for communication and sensing. We assume that uniform linear arrays (ULAs) with half-wavelength separation, i.e., $d = \lambda/2$, where $\lambda = c/f_c$, c is the speed of light, and f_c is the carrier frequency, are employed for both transmission and reception. According to [17], we assume that sensing is performed using repeated time-frequency slots composed of K subcarriers and M OFDM symbols each. Within such slots, a sensing beam is activated beside a communication beam (for downlink communication towards a user) [18]. However, for jamming detection, we pick one ‘‘observation’’ within each slot, which refers to a vector containing the received OFDM symbols (right after the FFT processing at the sensing receiver) across the K subcarriers at time n .

With such a multibeam ISAC approach only a fraction of total power of the OFDM signal is designated to sensing purposes. The discrete-time transmitted signal in the k th subcarrier of at time n , can be written as [18]

$$\mathbf{x}[k, n] = \mathbf{w}_T[n]x_{k,n} \quad (1)$$

where $k = 1, \dots, K$, $n = 1, \dots, N$ with N the number of observations, and $\mathbf{w}_T[n] \in \mathbb{C}^{N_T \times 1}$ is the sensing beamforming vector used to map each modulation symbol, $x_{k,n}$, to the transmitting antennas. By considering a beam steering

approach and performing a normalization with respect to the effective isotropic radiated power (EIRP) $P_T G_T$, we express the beamforming vector as

$$\mathbf{w}_T[n] = \frac{\sqrt{\rho P_T G_T}}{N_T} \mathbf{a}_T(\theta_T^n) \quad (2)$$

where $\rho \in [0, 1]$ is the parameter used to control the fraction of the total power apportioned to the sensing direction, P_T is the transmit power, G_T is the transmit array gain along the beam steering direction, and $\mathbf{a}_T(\theta_T^n) \in \mathbb{C}^{N_T \times 1}$ is the steering vector along the sensing directions θ_T^n . In particular, the steering vector for the considered ULA can be expressed as

$$\mathbf{a}_T(\theta_T^n) = \left[1, e^{i\pi \sin(\theta_T^n)}, \dots, e^{i\pi(N_T-1) \sin(\theta_T^n)} \right]^\top. \quad (3)$$

For generality and to facilitate jamming detection in an unknown environment, we assume the interval between two consecutive observations exceeds the channel’s coherence time. This results in different channel realizations for the sensing receiver with each observation. Additionally, the characteristics of both the target and jammer may vary across observations; for instance, their positions relative to the BS may change.

A. Jammer Model

A deceptive jammer in radar systems is a sophisticated ECM designed to mislead radar operations by transmitting false signals. These jammers create fake targets or alter the perceived location and speed of actual targets, confusing the radar’s tracking and detection capabilities. The most efficient way to implement a deceptive jammer consists of using a DRFM. It is a high-speed, analog-to-digital converter and storage system that provides the capability to sample, process, and playback radio frequency (RF) signals with minimum loss of fidelity. With these capabilities, the jammer can rapidly obtain pertinent data and formulate an effective strategy. For instance, in a hypothetical 5G NR network where ISAC is performed using the physical downlink shared channel-demodulation reference signal (PDSCH-DMRS), also designated as the pilot, the jammer may be able to access the primary and secondary synchronization signals in order to obtain the physical cell identity. The cell ID comprises data regarding the initialization of the PDSCH-DMRS. Consequently, the jammer is aware of the resource elements (REs) where the PDSCH-DMRS is transmitted and what symbols it is composed of, thus facilitating the transmission of a delayed version of the pilot towards the BS.

Let us consider a deceptive jammer capable of mimicking the signal transmitted by the BS and injecting a false delay into the received signal with the aim of falsifying the BS’s estimated location of the target. It can quickly obtain this information and plan its response accordingly. Specifically, this study assumes that the jamming attack occurs in the n th observation and k th subcarrier, using the same symbols $x_{k,n}$

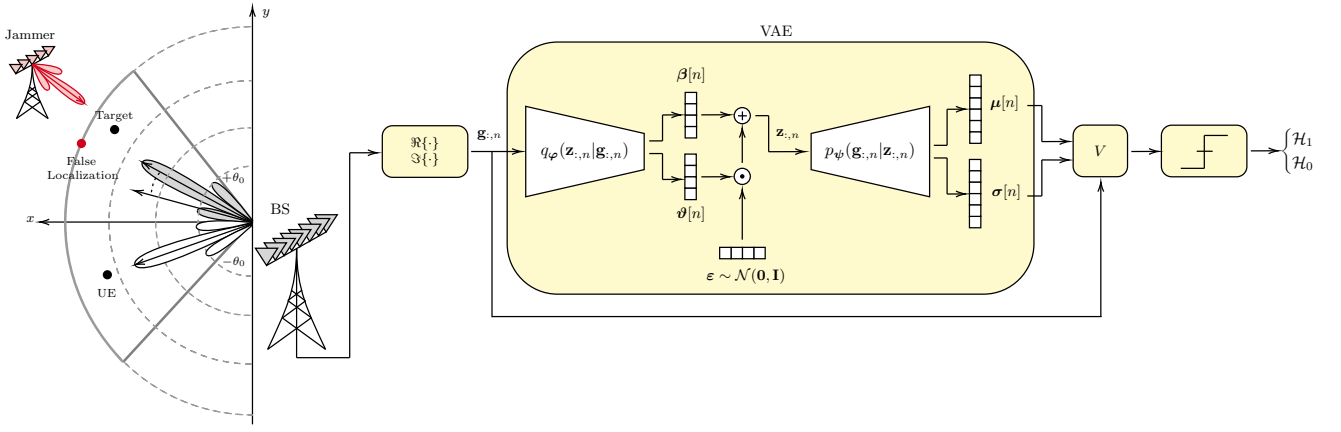


Fig. 1. The monostatic OFDM ISAC scheme in presence of a jammer: an illustration of the data gathering process and decision making. The latent variable inside the VAE is obtained using the well-known reparameterization trick $\mathbf{z}_{:,n} = \boldsymbol{\beta}[n] + \boldsymbol{\vartheta}[n] \cdot \boldsymbol{\epsilon}$, where $\mathbf{c} \cdot \mathbf{d}$ is the element-wise product between the two vectors \mathbf{c} and \mathbf{d} .

transmitted by the BS. This represents a worst-case scenario where the radar receiver is completely misled.¹

The jammer comprises a transmitter antenna array with N_J elements arranged in an ULA with half-wavelength separation and adopts OFDM modulation with K subcarriers. Therefore, its signal can be written as

$$\tilde{\mathbf{x}}[k, n] = \mathbf{w}_J[n] x_{k,n} e^{-i2\pi k \Delta f \tau_f^n} \quad (4)$$

where Δf is the subcarrier spacing, $\mathbf{w}_J[n] \in \mathbb{C}^{N_J \times 1}$ is the jammer beamforming vector, and τ_f^n is the false delay introduced by the jammer. The beamforming vector can be expressed as

$$\mathbf{w}_J[n] = \frac{\sqrt{P_J G_J}}{N_J} \mathbf{a}_J^*(\theta_J^n) \quad (5)$$

where P_J is the jammer signal power, G_J is the array gain along the beam steering direction, and $\mathbf{a}_J(\theta_J^n) \in \mathbb{C}^{N_J \times 1}$ is the steering vector.

B. Received Signal at the BS

Let us assume the presence of a point-like target within the sensing beam. The received signal is processed by a typical OFDM receiver [18], such that the vector $\mathbf{y}[k, n] \in \mathbb{C}^{N_R \times 1}$ of the received modulation symbols at each antenna after the fast Fourier transform (FFT) block is

$$\mathbf{y}[k, n] = \mathbf{H}[k, n] \mathbf{x}[k, n] + \tilde{\mathbf{H}}[k, n] \tilde{\mathbf{x}}[k, n] + \boldsymbol{\nu}[k, n] + \mathbf{m}[k, n] \quad (6)$$

where $\mathbf{H}[k, n] \in \mathbb{C}^{N_R \times N_T}$ is the channel matrix between the target and the BS for the k th subcarrier in the n th observation, $\tilde{\mathbf{H}}[k, n] \in \mathbb{C}^{N_R \times N_J}$ is the channel matrix between the BS and the jammer, $\boldsymbol{\nu}[k, n] \in \mathbb{C}^{N_R \times 1}$ is the vector whose elements represent the self-interference due to imperfect Tx–Rx isolation at each receiving antenna, and $\mathbf{m}[k, n] \sim \mathcal{CN}(\mathbf{0}, \sigma_N^2 \mathbf{I}_{N_R})$ is the noise power at the sensing receiver. Let us remark that, in absence of the jammer, the second term in (6) is zero.

¹For example, if sensing is performed using pilot symbols the possibility that the jammer might know $x_{k,n}$ is not unlikely.

The BS-target-BS channel matrix can be written as [18]²

$$\mathbf{H}[k, n] = \alpha_t^n e^{i\phi_t^n} e^{-i2\pi k \Delta f \tau_t^n} \mathbf{a}_R(\theta_t^n) \mathbf{a}_T^T(\theta_t^n) \quad (7)$$

where α_t^n , ϕ_t^n , τ_t^n , θ_t^n are the attenuation, phase, delay, and angle of arrival (AoA)/angle of departure (AoD) of the target for the n th observation, respectively.

The gain α_t^n includes the attenuation along the BS-target-BS path, that is calculated as

$$\alpha_t^n = \sqrt{\frac{c^2 \sigma_{\text{RCS}}^n}{(4\pi)^3 f_c^2 (r_t^n)^4}} \quad (8)$$

where r_t^n is the distance between the target and the BS in the n th observation, and σ_{RCS}^n is its radar cross-section (RCS). The target RCS is assumed to adhere to the Swerling I model, i.e., $\sigma_{\text{RCS}}^n \sim \exp(\bar{\sigma}_{\text{RCS}})$.

The jammer-BS channel matrix, instead, can be written as

$$\tilde{\mathbf{H}}[k, n] = \alpha_J^n e^{i\phi_J^n} e^{-i2\pi k \Delta f \tau_J^n} \mathbf{a}_R(\theta_{\text{BS},J}^n) \mathbf{a}_J^T(\theta_{J,\text{BS}}^n) \quad (9)$$

where α_J^n is the channel attenuation given by the path-loss equation, ϕ_J^n is the phase shift, and τ_J^n is the delay of the direct path. Furthermore, $\theta_{\text{BS},J}^n$ and $\theta_{J,\text{BS}}^n$ are the AoA and AoD of the line-of-sight (LOS) path.

Regarding the self-interference term in (6), each element of vector $\boldsymbol{\nu}[k, n]$ can be interpreted as the signal scattered by a static target located very close to the receiver [18]. Hence,

$$\boldsymbol{\nu}[k, n] = \alpha_{\text{SI}}^n x_{k,n} [e^{i\phi_{\text{SI},1}^n}, \dots, e^{i\phi_{\text{SI},N_R}^n}]^T \quad (10)$$

where α_{SI}^n is the self-interference attenuation and is the same for all receiving antennas, and $[\phi_{\text{SI},1}^n, \dots, \phi_{\text{SI},N_R}^n]$ are the phase shifts at the antennas.

²In this work we do not consider the Doppler effect for brevity but its presence can be included in the system and jammer models without altering the operating principle of the jammer detector.

C. Processing at the Base Station

Let us consider the vector of received symbols obtained from (6), $\mathbf{y}[k, n]$, and let us assume a specific sensing direction such that $\theta_R^n = \theta_T^n$. Spatial combining is then performed using the receiving beamforming vector as

$$\mathbf{w}_R[n] = \mathbf{a}_R^*(\theta_R^n) = \left[1, e^{-i\pi \sin(\theta_R^n)}, \dots, e^{-i\pi(N_R-1) \sin(\theta_R^n)} \right]^T.$$

This results in the formation of a grid of received symbols, where each element $y_{k,n}$ is obtained by taking the inner product between the receiving beamforming vector $\mathbf{w}_R[n]$ and the vector of the symbols received at each antenna $\mathbf{y}[k, n]$, i.e., $y_{k,n} = \mathbf{w}_R^T[n] \mathbf{y}[k, n]$. Then, reciprocal filtering is performed, which consists of an element-wise division between the received and the transmitted grids to remove the dependence on the transmitted symbols, yielding $g_{k,n} = y_{k,n}/x_{k,n}$. Considering the n th observation, we have

$$\begin{aligned} g_{k,n} &= \mathbf{w}_R^T[n] \mathbf{H}[k, n] \mathbf{w}_T[n] \\ &+ \mathbf{w}_R^T[n] \tilde{\mathbf{H}}[k, n] \mathbf{w}_J[n] e^{-i2\pi k \Delta f \tau_i^n} \\ &+ \frac{\mathbf{w}_R^T[n] \boldsymbol{\nu}[k, n]}{x_{k,n}} + \frac{\mathbf{w}_R^T[n] \mathbf{m}[k, n]}{x_{k,n}} \end{aligned} \quad (11)$$

where the second term is the signal injected by the jammer into the BS receiver to deceive sensing. Finally, for the sake of jamming detection, the real and imaginary parts of $g_{k,n}$ are split and arranged in a matrix $\mathbf{G} \in \mathbb{C}^{2K \times N}$, whose n th column is

$$\mathbf{g}_{:,n} = [\Re\{g_{0,n}\}, \dots, \Re\{g_{K,n}\}, \Im\{g_{0,n}\}, \dots, \Im\{g_{K,n}\}]^T.$$

III. VARIATIONAL AUTOENCODER

In this section, we introduce a variational Bayesian approach to detect the presence of the deceptive jammer introduced in Section II-A. We begin our analysis by observing that the system model in (11), in the absence of a jammer (i.e., when the second term is zero), can be interpreted as a latent model for the generation of $g_{k,n}$. Our initial objective is to learn the latent space generated by the system under no-jammer conditions by means of a variational autoencoder. Subsequently, we perform jamming detection based on the premise that the presence of a jammer will significantly alter the latent space, rendering it markedly different from the one identified in a jammer-free environment.

A. Variational autoencoder

VAE is a popular approach for unsupervised learning of generative latent models exploiting the power of neural networks [16]. In other words, it is a modern formulation of the variational inference (VI) framework, where the goal is to provide a good approximation for the posterior distribution $p_\psi(\mathbf{Z}|\mathbf{G})$ of the latent variables $\mathbf{Z} = \{\mathbf{z}_{:,n}\}_{n=1}^N$ given the observed data \mathbf{G} and with parameters ψ [19]. Assuming that the observations in \mathbf{G} are independent, we aim to find $p_\psi(\mathbf{z}_{:,n}|\mathbf{g}_{:,n})$. Since the posterior cannot be directly computed due to the intractability of the marginal likelihood, VI provides an approximate distribution $q_\varphi(\mathbf{z}_{:,n}|\mathbf{g}_{:,n})$ with parameters φ .

In particular, the best approximation can be computed by minimizing the following Kullback-Leibler divergence

$$\begin{aligned} D_{\text{KL}}(q_\varphi(\mathbf{z}_{:,n}|\mathbf{g}_{:,n})||p_\psi(\mathbf{z}_{:,n}|\mathbf{g}_{:,n})) &= \\ &- \mathbb{E}_{q_\varphi(\mathbf{z}_{:,n}|\mathbf{g}_{:,n})} \left[\ln \frac{p_\psi(\mathbf{g}_{:,n}, \mathbf{z}_{:,n})}{q_\varphi(\mathbf{z}_{:,n}|\mathbf{g}_{:,n})} \right] + \ln p_\psi(\mathbf{g}_{:,n}) \end{aligned} \quad (12)$$

or, equally, by maximizing the evidence lower bound (ELBO)

$$\mathcal{L}(\psi, \varphi, \mathbf{g}_{:,n}) = \mathbb{E}_{q_\varphi(\mathbf{z}_{:,n}|\mathbf{g}_{:,n})} \left[\ln \frac{p_\psi(\mathbf{g}_{:,n}, \mathbf{z}_{:,n})}{q_\varphi(\mathbf{z}_{:,n}|\mathbf{g}_{:,n})} \right]. \quad (13)$$

VAEs provides a stochastic VI solution aiming to maximize the $\mathcal{L}(\psi, \varphi, \mathbf{g}_{:,n})$ by means of gradient-based optimization.

Let us now assume the following prior distributions

$$p_\psi(\mathbf{g}_{:,n}|\mathbf{z}_{:,n}) \sim \mathcal{N}(\boldsymbol{\mu}[n], \boldsymbol{\sigma}^2[n] \mathbf{I}_{2K}), \quad (14)$$

$$p(\mathbf{z}_{:,n}) \sim \mathcal{N}(\mathbf{0}, \mathbf{I}_L), \quad (15)$$

$$q_\varphi(\mathbf{z}_{:,n}|\mathbf{g}_{:,n}) \sim \mathcal{N}(\boldsymbol{\beta}[n], \boldsymbol{\vartheta}^2[n] \mathbf{I}_L). \quad (16)$$

The choice of Gaussian priors for the latent space has many benefits: (i) the Gaussian distribution is mathematically convenient due to its properties, such as admitting a closed-form expression for the Kullback-Leibler divergence, which is essential for the VAE's optimization process; (ii) thanks to the central limit theorem, Gaussian priors are a natural and generalizable choice for modeling the latent space of diverse datasets; (iii) empirically, Gaussian priors have been shown to produce smooth and continuous latent spaces, which are desirable for generative tasks [16]. After proper manipulations, the ELBO can be written as

$$\begin{aligned} \mathcal{L}(\psi, \varphi, \mathbf{g}_{:,n}) &= -D_{\text{KL}}(q_\varphi(\mathbf{z}_{:,n}|\mathbf{g}_{:,n})||p(\mathbf{z}_{:,n})) \\ &+ \mathbb{E}_{q_\varphi(\mathbf{z}_{:,n}|\mathbf{g}_{:,n})} [\ln p_\psi(\mathbf{g}_{:,n}|\mathbf{z}_{:,n})]. \end{aligned} \quad (17)$$

Adopting the reparameterization trick proposed in [16], considering the prior distributions in (14), (15), and (16), it is possible to obtain a differentiable formulation for the ELBO, i.e.,

$$\begin{aligned} \mathcal{L}(\psi, \varphi, \mathbf{g}_{:,n}) &= \frac{1}{2} \sum_{l=1}^L (1 + \ln \vartheta_l^2[n] - \beta_l^2[n] - \vartheta_l^2[n]) \\ &- \underbrace{\frac{1}{2} \sum_{k=1}^{2K} \left(\ln 2\pi + \ln \sigma_k^2[n] + \frac{(g_{k,n} - \mu_k[n])^2}{\sigma_k^2[n]} \right)}_V \end{aligned} \quad (18)$$

where $V = -\mathbb{E}_{q_\varphi(\mathbf{z}_{:,n}|\mathbf{g}_{:,n})} [\ln p_\psi(\mathbf{g}_{:,n}|\mathbf{z}_{:,n})]$ is the reconstruction probability that will be used for jamming detection [20].

Fig. 1 encloses a schematic representation of a VAE. The function $q_\varphi(\mathbf{z}_{:,n}|\mathbf{g}_{:,n})$ serves as a probabilistic encoder that, given an input $\mathbf{g}_{:,n}$, generates a distribution over the possible values of $\mathbf{z}_{:,n}$ from which $\mathbf{g}_{:,n}$ could have been produced. Similarly, $p_\psi(\mathbf{g}_{:,n}|\mathbf{z}_{:,n})$ functions as a probabilistic decoder, producing a distribution over the possible values of $\mathbf{g}_{:,n}$ given $\mathbf{z}_{:,n}$. Thus, $\boldsymbol{\mu}[n]$, $\boldsymbol{\sigma}[n]$, $\boldsymbol{\beta}[n]$, and $\boldsymbol{\vartheta}[n]$ are the outputs of the encoder and decoder neural networks, whose weights are denoted by ψ and φ , respectively.

B. Anomaly detection

The VAE, trained on echoes captured in absence of a jammer, seeks to learn the latent variables that better represent the channel in presence of a target. Thus, after the training, if the VAE is fed with a vector $\mathbf{g}_{:,n}$ corresponding to the manipulated received signal in presence of a jammer, it provides an anomalous value for $\mathcal{L}(\psi, \varphi, \mathbf{g}_{:,n})$. Specifically, when the jammer is present results in significantly high values of the reconstruction probability V . Therefore, based on such considerations, we propose an anomaly detector that employs as metric the reconstruction probability, i.e.,

$$V \underset{\mathcal{H}_0}{\overset{\mathcal{H}_1}{\gtrless}} \omega. \quad (19)$$

Hypothesis \mathcal{H}_1 corresponds to the presence of a jammer, while the null hypothesis, \mathcal{H}_0 , corresponds to its absence. The thresholds ω is obtained by setting the false alarm probability $p_{\text{FA}} = (V > \omega | \mathcal{H}_0)$, where the null distribution is calculated via histogram-based probability density function estimation.

IV. NUMERICAL RESULTS

In this section, we evaluate the performance of the proposed solution and compare it with that of a conventional AE. For all the simulations, 5G new radio (NR) signals compliant with 3GPP Technical Specification in [21] are considered. According to the 5G NR standard, we employed a carrier frequency of $f_c = 28$ GHz, an EIRP $P_T G_T = 13$ dBW, subcarrier spacing $\Delta f = 120$ kHz, number of antennas $N_T = N_R = 50$, and the number of subcarriers used for the radar set to $K = 500$. In addition, a quadrature phase shift keying (QPSK) modulation alphabet is used for the generation of the OFDM signal, and the parameter ρ is set to 0.5. As shown in Fig. 1, the system scans the environment in the range $[-\theta_0, \theta_0]$, with $\theta_0 = 60^\circ$ and a beamwidth $\Delta\Theta = 5.3^\circ$ at -10 dB gain relative to the beam direction. Therefore, the number of step to cover the entire range is $N_{\text{step}} = \lceil \frac{2\theta_0}{\Delta\Theta} \rceil = 23$.

The self-interference attenuation α_{SI} is computed using the signal-to-self interference ratio (SSIR) defined as $\text{SSIR} = (\alpha_t^n / \alpha_{\text{SI}}^n)^2 = 20$ dB. The mean RCS is $\bar{\sigma}_{\text{RCS}} = 1 \text{ m}^2$, and the noise power spectral density is $N_0 = k_B T_0 F$, where $k_B = 1.38 \cdot 10^{-23} \text{ JK}^{-1}$ is the Boltzmann constant, $T_0 = 290 \text{ K}$ is the reference temperature, and $F_{\text{dB}} = 8 \text{ dB}$ is the receiver noise figure.

A. Algorithm's parameters

The VAE's encoder comprises a deep feed-forward neural network architecture, with the input layer receiving the normalized vector $\mathbf{g}_{:,n} \in \mathbb{R}^{2K \times 1}$, which has unit modulus. Following this, the encoder employs 5 hidden layers with 728, 256, 64, 32, and 10 neurons each, respectively. The encoder outputs two vectors, $\beta[n]$ and $\vartheta[n]$, each having a latent dimension of $L = 10$. The decoder takes the latent variable $\mathbf{z}_{:,n} = \beta[n] + \vartheta[n] \cdot \epsilon$ as input, where $\epsilon \sim \mathcal{N}(\mathbf{0}, \mathbf{I}_L)$. The decoder's architecture mirrors that of the encoder, producing the vectors $\boldsymbol{\mu}[n] \in \mathbb{R}^{2K \times 1}$ and $\boldsymbol{\sigma}[n] \in \mathbb{R}^{2K \times 1}$ as output. Each hidden layer employs the rectified linear unit (ReLU)

activation function, except for the layers computing $\beta[n]$ and $\vartheta[n]$, which employ a linear activation function. Since the input is normalized with unit modulus, the output layer for $\boldsymbol{\mu}[n]$ adopts the hyperbolic tangent activation function. Training is conducted using the Adagrad optimizer with learning rate $\eta = 0.005$, for $N_{\text{epoch}} = 4000$ epochs, and batch size $N_{\text{bs}} = 460$. The training objective is to minimize the negative ELBO, which is defined in (18).

To validate our VAE-based approach, we compare its performance with a conventional AE. The AE's encoder also employs a feed-forward deep neural network architecture, comprising 7 hidden layers with 728, 512, 256, 128, 64, 32, and 10 neurons each, respectively, where 10 denotes the bottleneck dimension. The decoder mirrors the encoder's architecture, giving as output the reconstructed vector $\hat{\mathbf{g}}_{:,n}$. Each hidden layer employs the ReLU activation function, while the output layer uses the hyperbolic tangent activation function. The AE is trained using the Adagrad optimizer with learning rate $\eta = 0.001$, over $N_{\text{epoch}} = 2000$ epochs, and a batch size of $N_{\text{bs}} = 200$. The loss function used for the training is the mean squared error (MSE).

For both training and validation, we use a matrix $\mathbf{G} \in \mathbb{R}^{2K \times N}$ with $N = 57.5 \cdot 10^3$ observations. Specifically, 80% of the observations are used for training, and the remaining 20% for validation. Both the VAE and AE architectures were selected after extensive parameter searches to achieve their optimal performance. To obtain a comprehensive training set that enables the VAE to learn a general representation of the latent space, we assume that independent observations are collected across various environments. Specifically, we assume that for each observation, the target position and the parameters related to the channel realization between the target and the BS are generated according to the following distributions:

$$\phi_t^n, \phi_{\text{SI},1}, \dots, \phi_{\text{SI},N_R} \sim \mathcal{U}(0, 2\pi), \quad (20)$$

$$r_t^n \sim \mathcal{U}(20, 85), \quad (21)$$

$$\theta_t^n, \theta_{\text{BS},J}^n \sim \mathcal{U}[\theta_T^n - \Delta\Theta, \theta_T^n + \Delta\Theta]. \quad (22)$$

For the n th observation, the direction of the BS' beam is set according to

$$\theta_T^n = \theta_R^n = -\theta_0 + \text{mod}(n - 1, N_{\text{step}})\Delta\Theta \quad (23)$$

where $\text{mod}(a, b)$ is the modulo operator which returns the remainder of the division between the two positive numbers a and b .

To evaluate the efficacy of the anomaly detector, the input for the test is a matrix comprising 4600 observations. Of these, 2300 represent instances where only the target is present, while the remaining observations include both the target and the jammer. Also for the test dataset we assume that, for each observation, the target position and the parameters related to the channel realization between the target and the BS are generated according to (20), (21), and (22), while the parameters related to the jammer are generated according to $\phi_J^n \sim \mathcal{U}(0, 2\pi)$, $\theta_J^n \sim \mathcal{U}(0, 2\pi)$, and $\theta_{J,\text{BS}}^n \sim \mathcal{U}[\theta_J^n -$

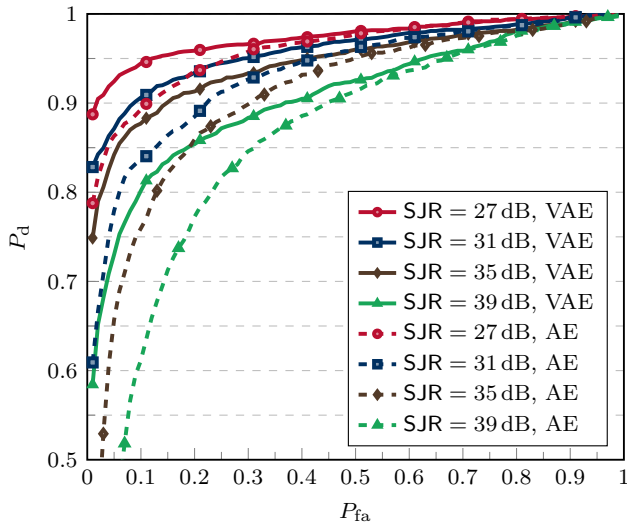


Fig. 2. ROC curves of the proposed VAE and the conventional AE for different SJR values.

$\Delta\Theta_j, \theta_j^n + \Delta\Theta_j]$, where $\Delta\Theta_j = 14^\circ$. The jammer is equipped with $N_j = 10$ antennas.

B. Impact of SJR

In this subsection, the performance of the proposed jamming detection method varying the SJR, is studied. The SJR is defined as the ratio between the EIRP of the legitimate signal and that of the jammer signal, i.e.,

$$\text{SJR} = \frac{\rho P_T G_T}{P_J G_J}. \quad (24)$$

The test is performed assuming the jammer is in a fixed position, i.e., $r_j^n = r_j = 90$ m, implying that the jammer is attempting to deceive the BS by staying outside its coverage area. For each observation, the injected false delay is set to $\tau_f^n = 0.17 \mu\text{s}$, corresponding to a false distance of 50 m. Fig. 2 shows the ROC curves for different SJR values for both the proposed VAE and the conventional AE. Considering a false alarm probability $P_{fa} = 0.05$, the VAE achieves a detection probability $P_d = 0.93$ for $\text{SJR} = 27$ dB. However, when the jammer's transmit power is significantly lower than BS's sensing power, the detection performance deteriorates. Moreover, from Fig. 2 it is evident that the VAE outperforms the conventional AE for each of the SJR values. The best performance produced by the VAE with regard to AE are caused by the difference between reconstruction probability and reconstruction error. The latent variables in a VAE are stochastic, whereas in autoencoders, they are defined by deterministic mappings. As the VAE employs a probabilistic encoder to model the distribution of latent variables rather than the variables themselves, it is able to account for the variability of the latent space through the sampling process. This increases the expressive power of the VAE in comparison to the autoencoder, as it is capable of capturing differences in

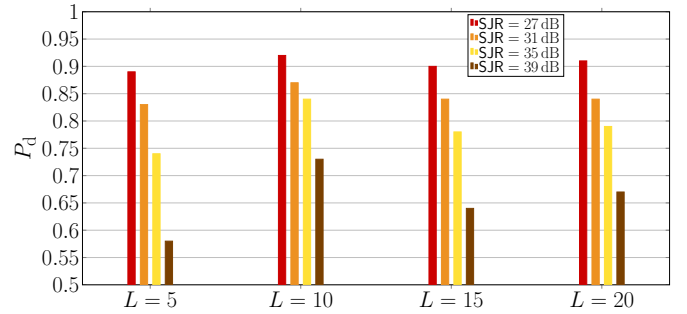


Fig. 3. Probability of detection P_d for different latent space dimensions, L , and SJR values, with a false alarm probability $P_{fa} = 0.05$.

variability even when normal and anomalous data share the same mean value [20].

C. Latent space dimension

Finally, we assess the impact of the latent space dimension hyperparameter, L , on the VAE's detection performance. Fig. 3 shows the probability of detection P_d , for different SJR values and latent space dimensions 5, 10, 15 and 20, with a false alarm probability $P_{fa} = 0.05$. Typically, setting a low latent space dimension prevents the VAE from capturing all the trends and variations in the training observations. Conversely, high values of L tend to keep the regularization term $D_{\text{KL}}(q_{\varphi}(\mathbf{z}_{:,n}|\mathbf{g}_{:,n})||p(\mathbf{z}_{:,n}))$ low during the training [22]. From Fig. 3, it is evident that setting $L = 10$ provides the best performance, even considering different SJR values. When $L = 5$, the VAE is unable to correctly learn the latent space, resulting in degraded detection probability. Similarly, for $L = 15$ and $L = 20$, the impact on the regularization term prevents the algorithm from fully exploiting its learning potential, leading to suboptimal performance. Therefore, both lower and higher values of L negatively affect the detection probability.

V. CONCLUSION

In this paper, we propose a novel framework for deceptive jamming detection in monostatic ISAC-OFDM systems. This framework leverages the received signal at the BS to detect the presence of a jammer capable of falsifying target localization. The proposed framework employs a VAE to learn a latent space representation of the echoes received from a target. Specifically, the reconstruction probability is utilized as a test statistic to detect the presence of a jammer. Our approach demonstrates significant detection performance, achieving a detection probability P_d of 93% for an SJR of 27 dB, and notably outperforming a properly trained conventional AE.

REFERENCES

- [1] Z. Wei, F. Liu, C. Masouros, N. Su, and A. P. Petropulu, "Toward multi-functional 6G wireless networks: Integrating sensing, communication, and security," *IEEE Commun. Mag.*, vol. 60, no. 4, pp. 65–71, Apr. 2022.

- [2] D. Tagliaferri, M. Mizmizi, S. Mura, F. Linsalata, D. Scazzoli, D. Badini, M. Magarini, and U. Spagnolini, "Integrated sensing and communication system via dual-domain waveform superposition," *IEEE Trans. Wireless Commun.*, vol. 23, no. 5, pp. 4284–4299, May 2024.
- [3] S. Mura, D. Tagliaferri, M. Mizmizi, U. Spagnolini, and A. Petropulu, "Waveform design for OFDM-based ISAC systems under resource occupancy constraint," in *IEEE Radar Conf. (RadarConf24)*, Denver, CO, USA, May 2024, pp. 1–6.
- [4] C. Zhang, L. Wang, R. Jiang, J. Hu, and S. Xu, "Radar jamming decision-making in cognitive electronic warfare: A review," *IEEE Sensors J.*, vol. 23, no. 11, pp. 11 383–11 403, Jun. 2023.
- [5] J. A. Zhang, M. L. Rahman, K. Wu, X. Huang, Y. J. Guo, S. Chen, and J. Yuan, "Enabling joint communication and radar sensing in mobile networks—a survey," *IEEE Commun. Surveys Tuts.*, vol. 24, no. 1, pp. 306–345, 2022.
- [6] T. Wild, V. Braun, and H. Viswanathan, "Joint design of communication and sensing for beyond 5G and 6G systems," *IEEE Access*, vol. 9, pp. 30 845–30 857, Feb. 2021.
- [7] Z. Huang, K. Wang, A. Liu, Y. Cai, R. Du, and T. X. Han, "Joint pilot optimization, target detection and channel estimation for integrated sensing and communication systems," *IEEE Trans. Wireless Commun.*, vol. 21, no. 12, pp. 10 351–10 365, Dec. 2022.
- [8] M. Greco, F. Gini, and A. Farina, "Radar detection and classification of jamming signals belonging to a cone class," *IEEE Trans. Signal Process.*, vol. 56, no. 5, pp. 1984–1993, May 2008.
- [9] S. Zhao, Y. Zhou, L. Zhang, Y. Guo, and S. Tang, "Discrimination between radar targets and deception jamming in distributed multiple-radar architectures," *IET Radar, Sonar & Navigation*, vol. 11, no. 7, pp. 1124–1131, Jul. 2017.
- [10] C. Xu, L. Yu, Y. Wei, and P. Tong, "Research on active jamming recognition in complex electromagnetic environment," in *IEEE Int. Conf. on Signal, Inf. and Data Processing (ICSIDP)*, Chongqing, China, Dec. 2019, pp. 1–5.
- [11] X. Wang, G. Zhang, X. Wang, Q. Song, and F. Wen, "ECCM schemes against deception jamming using OFDM radar with low global PAPR," *Sensors*, vol. 20, no. 7, p. 2071, Apr. 2020.
- [12] J. Sun, Y. Yuan, M. S. Greco, F. Gini, and W. Yi, "Anti-deception jamming power optimization strategy for multi-target tracking tasks in multi-radar systems," in *IEEE Int. Conf. on Acoustics, Speech and Signal Proc. (ICASSP)*. Seoul, Korea: IEEE, Apr. 2024, pp. 8941–8945.
- [13] L. Arcangeloni, E. Testi, and A. Giorgetti, "Detection of jamming attacks via source separation and causal inference," *IEEE Trans. Commun.*, vol. 71, no. 8, pp. 4793–4806, Aug. 2023.
- [14] E. Testi and A. Giorgetti, "Wireless network analytics for the new era of spectrum patrolling and monitoring," *IEEE Wireless Commun.*, pp. 1–7, May 2024.
- [15] Q. Lv, Y. Quan, W. Feng, M. Sha, S. Dong, and M. Xing, "Radar deception jamming recognition based on weighted ensemble CNN with transfer learning," *IEEE Trans. Geosci. Remote Sens.*, vol. 60, pp. 1–11, Nov 2021.
- [16] D. P. Kingma and M. Welling, "Auto-encoding variational bayes," *arXiv preprint arXiv:1312.6114*, 2013.
- [17] E. Favarelli, E. Matricardi, L. Pucci, W. Xu, E. Paolini, and A. Giorgetti, "Sensor fusion and resource management in MIMO-OFDM joint sensing and communication," *arXiv preprint arXiv:2312.07379*, 2023.
- [18] L. Pucci, E. Paolini, and A. Giorgetti, "System-level analysis of joint sensing and communication based on 5G new radio," *IEEE J. Sel. Areas Commun.*, vol. 40, no. 7, pp. 2043–2055, Mar. 2022.
- [19] M. D. Hoffman, D. M. Blei, C. Wang, and J. Paisley, "Stochastic variational inference," *Journal of Machine Learning Research*, vol. 14, no. 40, pp. 1303–1347, May 2013.
- [20] J. An and S. Cho, "Variational autoencoder based anomaly detection using reconstruction probability," *Special lecture on IE*, vol. 2, no. 1, pp. 1–18, 2015.
- [21] 5G, NR, *Physical Channels and Modulation*. 3GPP, Jul. 2020, vol. version 16.2.0 Release 16.
- [22] C. Doersch, "Tutorial on variational autoencoders," *arXiv preprint arXiv:1606.05908*, 2016.